Probing the topological surface state in Bi_2Se_3 thin films using temperature-dependent terahertz spectroscopy

Varun S. Kamboj[a], Angadjit Singh[a], Thierry Ferrus[b], Harvey E. Beere[a], Liam B. Duffy[c], Thorsten Hesjedal[c], Crispin H.W. Barnes[a] and David A. Ritchie[a]*

[a]*Cavendish Laboratory, University of Cambridge, J. J. Thomson Avenue, Cambridge CB3 0HE, United Kingdom;*

[b]*Hitachi Cambridge Laboratory, J. J. Thomson Avenue, Cambridge CB3 0HE, United Kingdom;*

[c]*Department of Physics, Clarendon Laboratory, University of Oxford, Oxford OX1 3PU, United Kingdom*

ABSTRACT: Strong spin-momentum coupling in topological insulators give rise to topological surface states, protected against disorder scattering by time reversal symmetry. The study of these exotic quantum states not only provides an opportunity to explore fundamental phenomenon in condensed matter physics such as the spin hall effect, but also lays the foundation for applications in quantum computing to spintronics. Conventional electrical measurements suffer from substantial bulk interference, making it difficult to clearly identify topological surface state from the bulk. We use terahertz time-domain spectroscopy to study the temperature-dependent optical behavior of a 23-quintuple-thick film of bismuth selenide (Bi_2Se_3) allowing the deconvolution of the surface state response from the bulk. The signatures of the topological surface state at low temperatures (< 30 K) with the optical conductance of Bi_2Se_3 exhibiting a metallic behavior are observed. Measurement of carrier dynamics, obtain an optical mobility, exceeding 2000 $cm^2/V•s$ at 4 K, indicative of a surface-dominated response. A scattering lifetime of ~0.18 ps and a carrier density of 6×10^{12} cm^{-2} at 4 K were obtained from the terahertz time-domain spectroscopy measurement. The terahertz conductance spectra reveal characteristic features at ~1.9 THz, attributed to the optical phonon mode, which becomes less prominent with falling temperature. The electrical transport measurements reveal weak antilocalization behavior in our Bi_2Se_3 sample, consistent with the presence of a topological surface state.

Keywords: topological insulators, bismuth selenide, terahertz spectroscopy, optical mobility, topological surface state, weak antilocalization.

Topological insulators (TIs) are a new class of materials that have an insulating bulk but possess a gapless conducting surface state arising from the non-trivial topology of the band structure[1]. The topological surface state (TSS) is 'robust' as it is protected against backscattering by spin-momentum locking and time reversal symmetry[1-4]. The surface state of a three-dimensional TI involves an odd number of Dirac cones in the surface Brillouin zone, guaranteed by the Z_2 topological invariant of the bulk[4,5]. The surface state of Bi_2Se_3 presents a particularly interesting case with a single Dirac cone on the surface[6-9], which can be described by strong spin orbit coupling[5,10] and which exhibits helical behavior[11], i.e., spin and translation momentum vectors are at fixed angles (90^0) to each other. These surface states have been proposed to have a wide range of applications from spintronics[1,7,12] to quantum computing[13]. In an ideal TI, the bulk does not contribute to charge transport and the conductivity is solely governed by surface carriers. However, the present generation of TIs, in particularly the chalcogenides of the $(Bi,Sb)_2(Se,Te)_3$ family, exhibit significant contributions from the bulk carriers to the net conductivity. The primary reason for this behavior is the doping due to Se or Te vacancies and anti-site defects[14], which are shifting the electrochemical potential close to the

conduction band. Furthermore, if the Fermi level crosses the bulk band near the surface, it can also lead to the formation of a two-dimensional electron gas (2DEG) in a quantum well, formed due to band bending near the surface. Such a 2DEG is limited to within ~20 nm of the surface[15,16] and appears alongside the TSS. The functionality of TIs as a viable material for novel technological applications requires unambiguous separation of the surface state response from the interfering bulk and quantum well states (QWSs). The TSS differs from the bulk states and QWSs in their topological origin, and hence display much higher scattering lifetime and mobilities, owing to their topological protection[3]. However, conventional electrical transport measurements face the difficultly of selectively probing the TSS, and distinguishing it from the bulk carrier contribution. Although angle-resolved photoemission spectroscopy (ARPES) can probe the TSS directly, its sensitivity is limited only to surface carriers, lacking high-energy resolution to resolve energy states near the Fermi level[17]. Recently, terahertz time-domain spectroscopy (THz-TDS) has been performed on $Bi_{1.5}Sb_{0.5}Te_{1.8}Se_{1.2}$ (BSTS)[18], but the observed response was a combination of surface and bulk contributions due to issues associated with defects and surface deterioration. In contrast, Bi_2Se_3 has a relatively stable surface with negligible reactivity to oxygen[19]. It would be highly desirable to have a technique which can detect and isolate the TSS response from the bulk contribution unambiguously, close to the Fermi level, with the capability to selectively address the TSS. Terahertz (THz) spectroscopy is a contact-free optical technique, used to probe the low-energy excitations in strongly correlated electron gases. In the THz (sub-millimeter) region, the frequency of the electromagnetic radiation is comparable to the carrier damping rate, rendering this technique particularly sensitive to study the TSS in TIs.

Here, we report the use of a broadband THz-TDS to unambiguously identify the TSS contribution, and to distinguish it from the bulk and QWS contributions, by measuring the THz transmittance of Bi_2Se_3 as a function of temperature. We extract the carrier scattering lifetime entirely from the phase of the THz signal at different temperatures, and further obtain the mobilities and carrier densities by purely optical means allowing us to fully characterize the TSS response. Our technique does not require an optical pump arrangement[50,51] conventionally used to obtain parameters such as scattering lifetime. Instead, it allows for a more straight-forward measurement of the equilibrium (non-photoexcited) material properties, especially relevant for TI-based electronic applications. We demonstrate a transition from a bulk-like response, dominant at high temperatures, to a metallic surface state response at low temperatures with the transition at ~30 K. Magneto-transport measurements reveal the value of α as 0.5, indicating that the observed response could originate from a coupled top and bottom TSS. This work provides fundamental insights into the carrier dynamics of the TSS and bulk carriers using a non-destructive method, enabling a technique to characterize future TI material system aimed at possible future applications.

RESULTS AND DISCUSSION

The complex optical transmission, $\tilde{T}(\omega) = T_1 + iT_2$ of a thin film allows the determination of parameters such as mobilities and carrier densities relevant to transport properties, where T_1 and T_2 are the real and imaginary components, respectively. The real and imaginary parts of the transmission are independent of each other, albeit being measured simultaneously. The imaginary part of the transmission is associated with the phase shift with respect to a reference substrate, and hence can be used to obtain the momentum relaxation time and mobility of carriers in the TI film. Moreover, the complex transmission obtained from the THz TDS can be used to deduce the THz conductance of Bi_2Se_3, which can be directly compared to the quasi-d.c. conductance obtained from electrical transport measurements. This makes THz-TDS a powerful tool to measure key material parameters related to TI thin films. A schematic of the optical arrangement is illustrated in Figure 1(a) and a detailed description is provided in the Methods section.

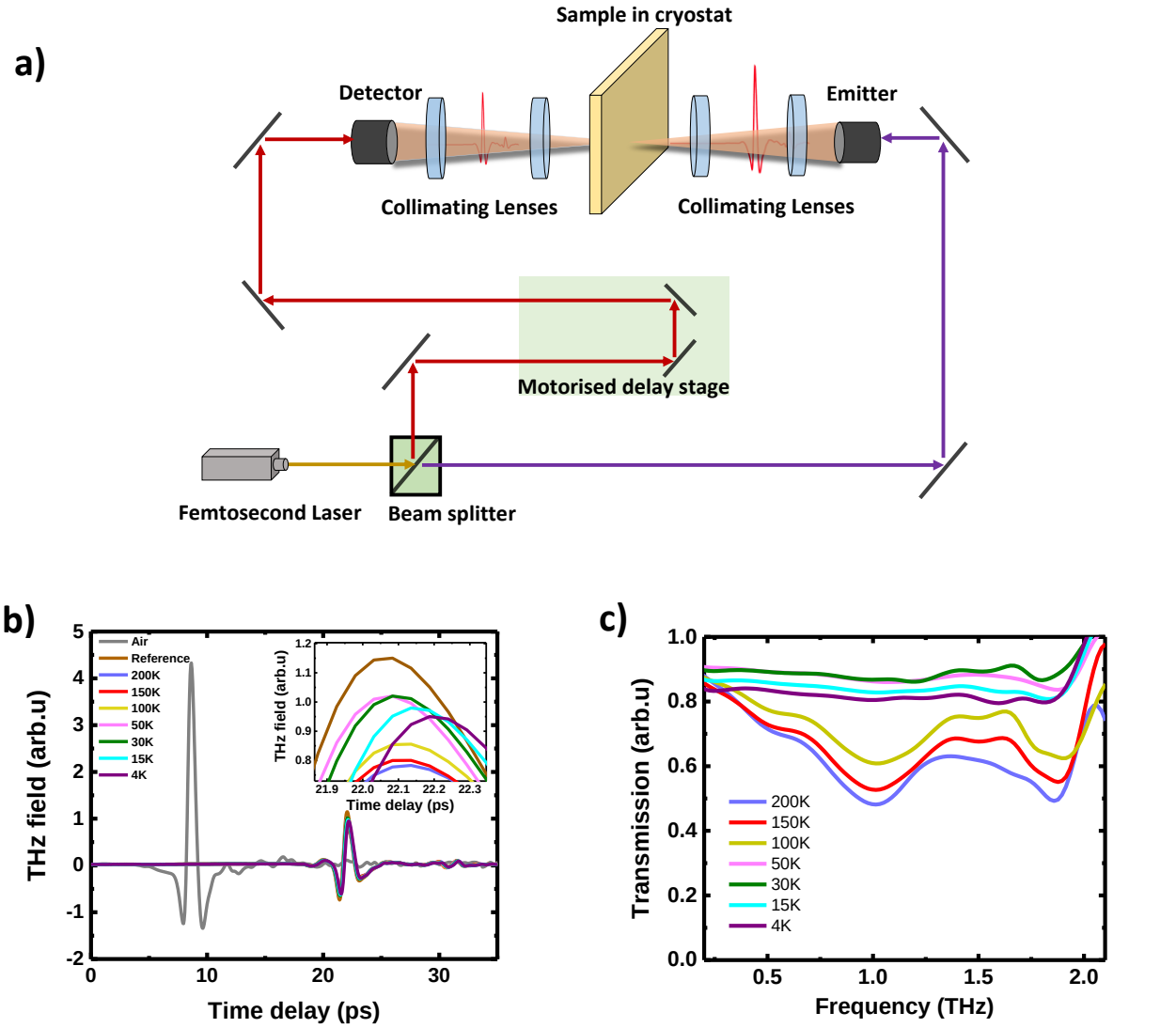

Figure 1. (a) Schematic of a THz-TDS optical setup. The light of a 60-mW pump laser of 90 fs duration, centered at 1560 nm, was split into two paths for THz generation (purple) and detection (red). (b) Time domain picosecond (ps) pulse response transmitted through air and a Bi_2Se_3 film of 23 QL (quintuple layer) at different temperatures. The inset shows a magnified pulse response transmitted through the Bi_2Se_3 film. The reference is transmission through (0001)-oriented sapphire substrate shown for 200 K. All the temperature measurements were performed in a cryostat with optical access with a base temperature of 4 K. (c) Normalized transmission amplitude spectra with respect to substrate at same temperature obtained from the Fourier transform of the temporal THz signal through Bi_2Se_3 from 4 K to 200 K.

The time-resolved THz transmission through the Bi_2Se_3 thin film was measured at various temperatures as shown in Figure 1b. The THz signal through the film shows an attenuated response and is displaced in time with respect to the signal through air. This signifies a change in the phase of the transmitted THz signal due to the refractive index and thickness of the sample, introduced in the path of the THz beam. We observe that the transmitted THz field intensity initially increases with reducing temperature down to 30 K, before decreasing with a further reduction in the temperature to 4 K (see inset in Figure 1b). To further probe this behavior, we extracted the transmission amplitude as shown in Figure 1c) from the Fourier transform of the primary transmitted pulse through Bi_2Se_3, normalized to the signal through the sapphire substrate at the same temperature (see Supplemental Material for THz temperature dependence of sapphire). We observe that the transmission initially increases with decreasing temperature up to 30 K, which explains the initial upsurge in the THz field intensity due to a reduced free carrier absorption in the film. However, below 30 K, the transmitted

intensity reduces as the temperature is reduced to 4 K, indicating the presence of two different states in Bi_2Se_3 with different properties and distinct spectral features. The transmission spectrum is characterized by a broad dip at around 1 THz (4.1 meV), which can be attributed to intersubband transitions in QWSs. The presence of the QWSs in thin film Bi_2Se_3 has already been confirmed by ARPES measurements in other Bi_2Se_3 studies[20,21]. The QWSs form via band bending (or from Se vacancies) near the surface and are described by a triangular potential well model, as discussed in a previous report[22], allowing us to assign the absorption feature at 1.0 THz to the so-called intersubband-band transition. The transmission spectra also show a strong dip at 1.9 THz (8 meV) depicting the optical phonon mode (α-phonon), which becomes weaker with reducing temperature, representing reduced electron-phonon scattering at low temperatures. The response observed in the transmission spectrum is in good agreement with previous studies on Bi_2Se_3[23,24]. Moreover, the spectral features show a strong temperature-dependent behavior and a systematic transition from bulk behavior to a surface-like response.

The THz conductance can be calculated using Tinkham's formula[25] (see Methods). Since the THz-TDS technique measures both the amplitude and phase of the signal, it is not necessary to employ the Kramers-Kronig transformation to obtain the optical conductivity. We observed that the THz conductance (Figure 2a) reduces with decreasing temperature down to 30 K, implying the freezing out of bulk charge carries in Bi_2Se_3. This further explains the initial upsurge observed in the transmission (Figure 1c) as the free carrier absorption is reduced in the Bi_2Se_3 film. We also identify the broad signature at 1 THz and the sharp peak at 1.9 THz as the contributions from the QWSs and the optical phonon, respectively, as discussed earlier. As the temperature decreases from 200 K to 4 K we expect a reduced contribution from the bulk and QWSs, thus leaving the TSS (consisting mainly of the top and bottom contributions in an extended thin film system) as the main contributor to the measured conductance values.

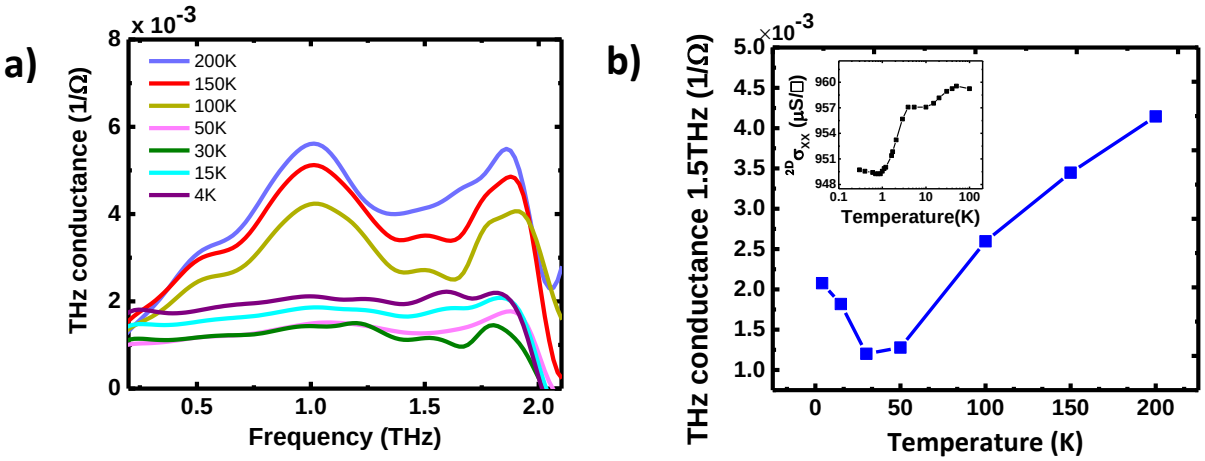

Figure 2. (a) The THz conductance spectra of Bi_2Se_3 showing distinct features at ~1 THz, corresponding to the QWSs intersubband transitions, and 1.9 THz referring to the optical phonon mode. (b) THz conductance at 1.5 THz as a function of temperature. The conductance first decreases and then increases with falling temperature, indicating the presence of two different phases at low and high temperatures. The inset shows the conductance obtained from the transport measurements, with a functional form similar to THz measurements, though showing a surface metallic response at ~1.2 K.

The diminishing QWSs (THz) response with reducing film thickness has been reported previously and was suggested to indicate a surface channel transport[23]. The THz conductance spectra confirm the emergence of TSS phenomena in Bi_2Se_3 below 30 K (Figure 2b). The conductance at 1.5 THz where the spectra is relatively flat shows an increase from ~1.20×10^{-3} Ω^{-1} to 2.07×10^{-3} Ω^{-1} (change of ~20 e^2/h), as the temperature is reduced from 30 K to 4 K, confirming the advent of a metal-like

surface behavior, characteristic of the TSS. The electrical conductance values rely on the Hall bar geometry; see Methods regarding the dimensions of the Hall bar. It is interesting to note that the electrical transport measurements (inset to Figure 2b) on Bi_2Se_3 also demonstrate a surface metallic response, though seen at a much lower temperature (~1.2 K) than observed through the optical THz measurements. This potentially highlights the well-known issue associated with trying to distinguish TSS contributions from a noisy background through transport measurements, especially for ultra-thin films[26]. The low frequency extrapolation of the THz conductance spectra should approach the d.c. conductance values obtained from standard transport measurements. However, it should be noted that standard transport measurements rely heavily on device geometry and processing, making it difficult to obtain a TSS response from the pristine surface of a TI. While we took all precautions to minimize any direct surface contact, the DI water involved in the device processing could react with the Bi_2Se_3 to form hydrogen selenide (leading to Se vacancies in the film) and bismuth hydroxide resulting in an overall n-type behavior of the film[22]. Even though this does not directly affect the TSS, the increased doping might make it more challenging to distinguish surface from bulk response. The THz conductance measurements, on the other hand, present an alternative way of obtaining the quasi-d.c. conductance behavior in TIs. It is worth mentioning that we rule out the contributions of QWSs to the metallic behavior of the THz conductance (Figure 2b), since we observe a diminishing QWSs response at ~1 THz (Figure 2a), which freezes out below 100 K and which is not observed at 50 K.

To further establish the distinct signature of the TSS at low temperatures we obtained the scattering lifetime and mobility of Bi_2Se_3 employing THz-TDS. Using Tinkham's equation for thin film[25] (see Methods) and substituting for the complex Drude conductivity as $\tilde{\sigma}(\omega) = \sigma_0/(1 - i\omega\tau)$, we obtain the following relationship between the imaginary and the real transmission: $Im.\{\tilde{T}(\omega)\}/Re.\{\tilde{T}(\omega)\} = -\omega\tau = \tan\phi$. Here, ϕ is the phase angle between the sample and substrate waveform, ω is the angular frequency and τ is the scattering lifetime for the carriers. Thus, the scattering lifetime can be directly obtained from the imaginary and the real part of the transmission, without the need of any further parameters. The imaginary part of the transmission spectra show the associated phase variations due to spectral features (QWSs and optical phonon) in the real transmission (Figure 3a). Plotting $\tan\phi$ as a function of frequency (Figure 3b) and fitting it with a linear regression, the slope yields the scattering lifetime (τ) and hence the mobility (μ) as a function of temperature, where $\mu = \tau e/m^*$. As a first-order approximation, the electron effective mass m^* in Bi_2Se_3 is 0.15 m_e, where m_e is the bare electron mass.[26,33,35,36,48]

Figure 3c shows the temperature-dependence of τ and μ from 200 K to 4 K. We obtained a scattering lifetime of τ = 0.18 ps at 4 K (inset to Figure 3c), and thus the mean-free path of surface electrons as $l = \tau \cdot v_F \approx 119$ nm, where v_F ($\approx 6.6 \pm 3 \times 10^5$ m/s) is the Fermi velocity of Bi_2Se_3 [7,23,27,48]. The scattering lifetimes of carriers exhibits a power law dependence of $\tau \sim T^{-1.4}$ at temperatures above 50 K, which is consistent with phonon scattering mechanism[28] as discussed before in Figure 2a. The plot of THz μ vs. T (Figure 3c) highlights two regimes: above 50 K, mobility drops gradually with temperature indicating that phonon scattering dominates any rise in the conduction due to increasing carrier density (n), resulting in the conduction being primarily bulk-dominated. Below 50 K, the mobility rises very rapidly demonstrating a metallic surface state response. Due to reduced phonon scattering and freezing of bulk carriers below 50 K, the TSS response becomes the dominant contribution to the measured conduction, thus explaining the sharp rise in mobility (and scattering lifetime).

It is interesting to note that the mobility shows a gradual reduction above 50 K, in contrast to its sharp rise below 50 K. This arises from a unique non-trivial property of TIs where a Dirac-like surface state co-exists with the bulk bands[3]. Although, increasing the temperature increases the surface scattering (τ decreases), the electronic relaxation from bulk to the TSS[29-31] states suppresses this increase of the surface scattering rate, hence resulting in a smaller gradient in mobility at high temperatures (>50 K). However, at low temperatures (<50 K) the electronic relaxation from the bulk to the TSS is

quenched[31], allowing a rapid change in the optical mobility. Such non-trivial behavior has been reported before in TIs, where electron relaxation from bulk to the surface suppresses the photo-induced surface scattering at high temperature[32]. The measured value of the surface state mobility at 4 K was 2124 $cm^2/V•s$ (with an effective mass of 0.15 m_e)[33] and ~220 $cm^2/V•s$ at 100 K, consistent with the literature values for TSS and bulk mobilities[26]. The mobilities obtained from the Hall measurements are plotted alongside the THz optical mobilities (Figure 3c). The THz and Hall mobilities are consistent at 100 K and above. The discrepancy below 100 K highlight the difficulty in identifying the TSS with respect to the bulk contribution, as the Hall measurements primarily show a bulk response, which is attributed to substantially high surface scattering even at low temperatures.[34]

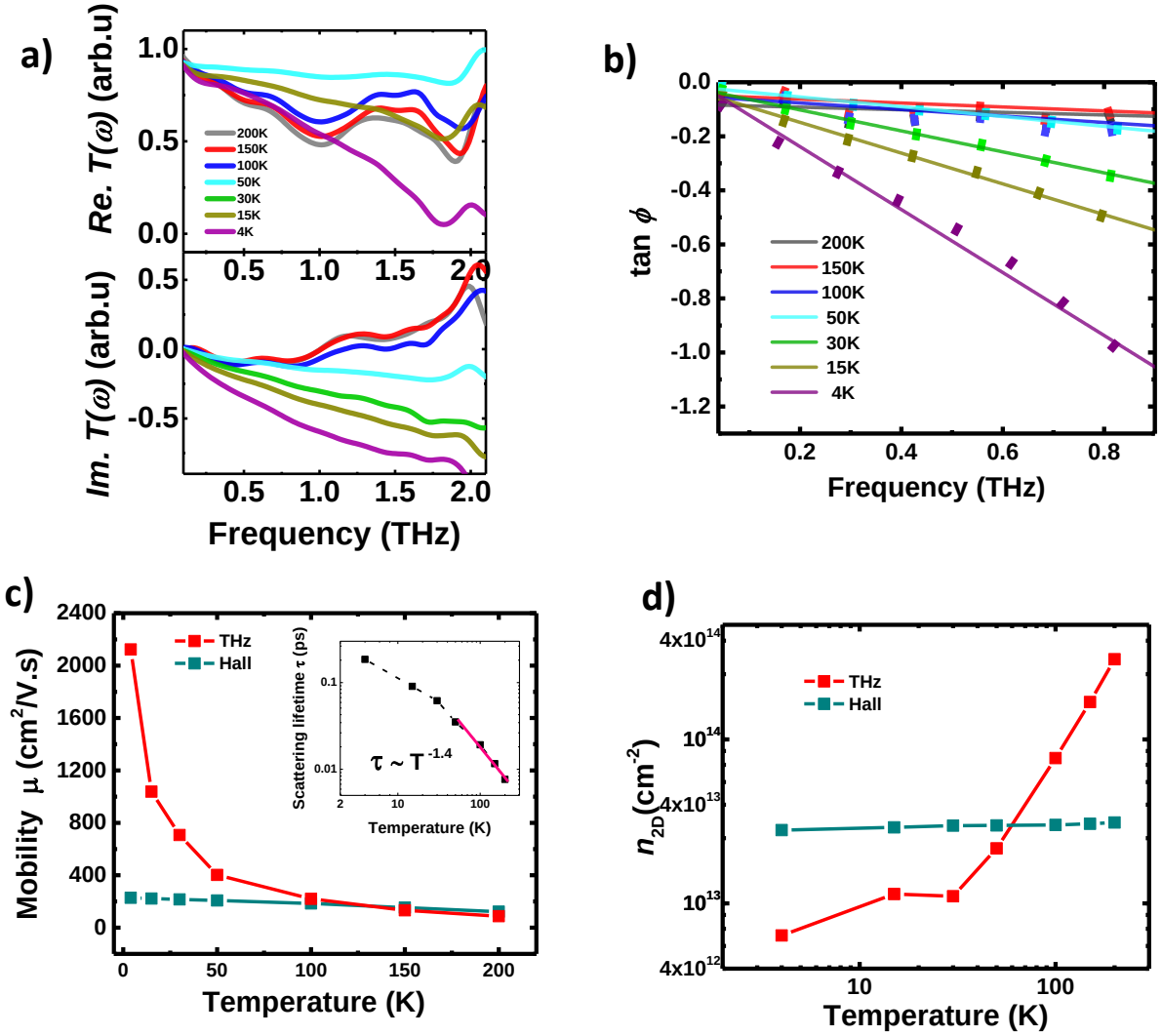

Figure 3. (a) Real and Imaginary transmission vs. frequency. The imaginary transmission reflecting the accompanying phase distortions in the real transmission (b) Plot of $\tan\phi$ vs. frequency. The solid lines represent the linear fit to each data set. The inset shows the real and imaginary parts of the complex transmission $\tilde{T}(\omega)$ used to obtain $\tan\phi$. (c) The plot of mobility μ vs. temperature obtained from the THz measurements (red curve) demonstrates a metallic surface state response below 50 K, and the Hall measurements (green curve) a predominantly bulk type response. The inset shows the scattering lifetime τ deduced from the THz-TDS. The solid line represents the power law dependence of $\tau \sim T^{-1.4}$, which suggests phonon scattering mechanism at temperatures above 50 K. (d) Sheet carrier density as a function of temperature deduced from the THz measurements (red curve) and Hall measurements (green curve).

The carrier concentration n_{TSS}, can be obtained using $G_{TSS} = G(\omega \to 0) = n_{TSS}.e.\mu$, yielding a value of $\sim 6 \times 10^{12} cm^{-2}$ at 4 K. This is consistent with the surface state carrier concentration measured by Brahlek *et al.*[35]; they obtained the surface carrier density to be $\sim 5 \times 10^{12} cm^{-2}$ from

Shubnikov–de Haas (SdH) oscillations, suggesting the TSS origin of the charge carriers in these measurements. Assuming a linear dispersion of the topological surface state, we estimated the position of the Fermi level, given by $E_F = \hbar v_F \sqrt{4\pi\, n_{TSS}}$ (where v_F is the Fermi velocity) to be ~ (0.38 ± 0.17) eV above the Dirac point. This value is consistent with the ARPES reports [6,15,16,38], further suggesting that the sheet carrier density obtained from the THz measurements is in fact representative of the surface electron density at 4 K. At a higher temperature of 50 K the quasi-Fermi level increases to 0.6 eV, possibly due to bulk-to-surface electron relaxation[32]. The THz optical carrier density (n_{2D}) rises with temperature (Figure 3d), indicating an increasing contribution from the bulk carriers to the measured conduction clearly observed above 50 K. This is in good agreement with bulk carrier densities of $\sim 5 \times 10^{14}$ cm^{-2} measured by He *et al.*[27] The carrier density obtained from Hall measurements show a predominantly bulk/ impurity response, possibly due to surface doping from the need for device processing[37] (see Supplemental Material for the Hall measurements and Methods for device processing). The measured THz sheet carrier density of TSS $n_{TSS} = {k_{F,TSS}}^2/(4\pi)$, yield a Fermi wave vector $k_{F,TSS}$ of 0.09Å^{-1} at 4 K and 0.11 Å^{-1} at 15 K, consistent with the ARPES values associated with topological surface bands on Bi_2Se_3 films. [6,15,16,38] This further confirms the TSS origin of the carrier densities and mobilities. It should be noted that our THz measurement stands out as a technique to probe both the surface and bulk states, though it is more surface-sensitive at higher frequencies due to a reduced skin depth.

More detailed electrical transport measurements were carried out on the 23 QL Bi_2Se_3 film employing a Hall bar geometry. They were fabricated using photolithography and Argon ion milling to define a mesa with a length-to-width (L/W) ratio of 5.25 when measured as shown in the inset to Figure 4a; see Methods regarding the device fabrication. A sharp increase in the conductivity is observed at low magnetic field, B, when increasing the temperature from 0.3 K to 100 K demonstrating weak antilocalization (WAL) behavior (Figure 4a). Such a phenomenon reflects both the Dirac nature of the surface states as well as the strong spin-orbit interaction in a TI material[39].

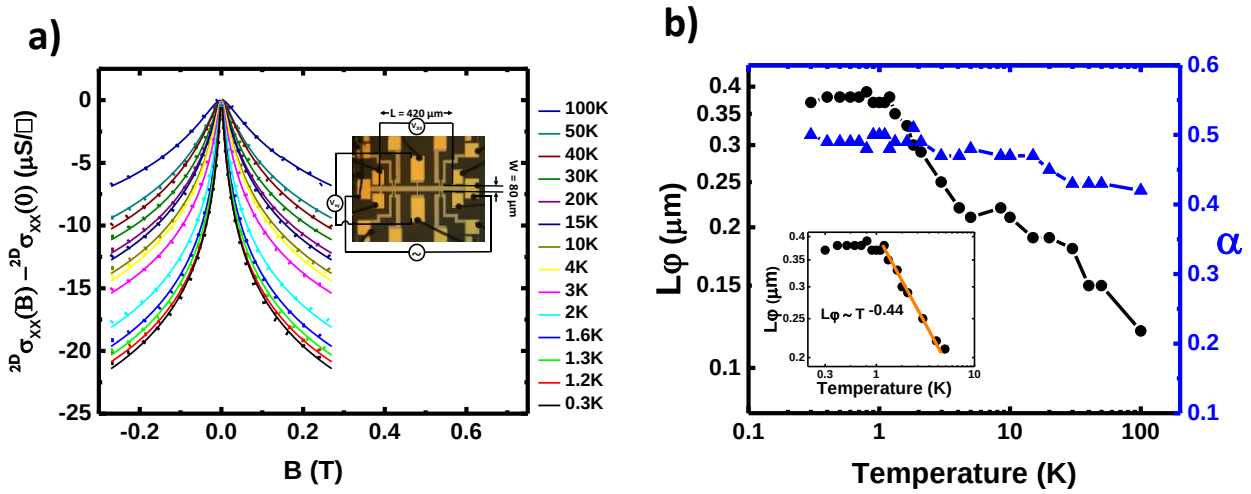

Figure 4. Weak antilocalization effect in Bi_2Se_3. (a) Normalized conductivity changes as a function of magnetic field measured at different temperatures. Each data set is fitted (solid line) to the HLN formula described in the text. The cusp in conductance is a characteristic feature of the WAL effect. (b) Plot of the fitted parameters L_φ and α as a function of temperature obtained from the WAL fit. The inset shows the power law fit of $L_\varphi \sim T^{-0.44}$, confirming that the observed WAL effect originates from the surface states.

In the presence of a perpendicular magnetic field, the time-reversed channels undergo destructive quantum interference resulting in a cusp in magnetoresistance. This behavior is described by the Hikami-Larkin-Nagaoka (HLN) equation[40] given as:

$$\Delta\sigma_{xx}^{2D} \equiv \sigma_{xx}^{2D}(B) - \sigma_{xx}^{2D}(0) = \alpha \frac{e^2}{2\pi^2 \hbar}\left[ln\left(\frac{\hbar}{4eBL_\varphi^2}\right) - \Psi\left(\frac{1}{2} + \frac{\hbar}{4eBL_\varphi^2}\right)\right] \quad (1)$$

where $\Delta\sigma_{xx}^{2D}$ indicates the normalized 2D sheet conductivity, B is the magnetic field perpendicular to the plane of the film, e is the electronic charge, $\hbar$ is the reduced Planck constant, Ψ is the digamma function, α is the number of topological surface modes (TSM), and L_φ is the phase coherence length.

Figure 4b shows the variation of α and L_φ as a function of temperature, extracted from the fit of the HLN equation to the WAL signal. We obtain a value for prefactor $\alpha \approx 0.5$, which remains largely unchanged from 0.3 K to around 15 K. Steinberg *et al.*[53] demonstrated that application of a gate voltage can vary α between 0.5 to 1 and hence it can be used phenomenologically as a measure of the top and bottom channel separation (with $\alpha \approx 1$, indicates decoupling of the top surface from the rest of the system). In this context, $\alpha \approx 0.5$ suggests that the top and the bottom TSS could be coupled in the Bi_2Se_3 film[53]. Another possible scenario is that the top surface is contributing significantly more to the WAL than the bottom surface, hence resulting in $\alpha \approx 0.5$. This might be due to a somewhat reduced phase coherence length, L_φ at the bottom interface, owing to the defects present at the TI-substrate interface[42,43], possibly also affected by the lattice mismatch between the Bi_2Se_3 and the substrate[43,52]. Beyond ~15 K, α starts to drop with temperature indicating increasing bulk interference[41]. The sharpness of the WAL cusp determines the phase coherence length, L_φ. This length characterizes phase coherent behavior of carriers before an inelastic scattering event, indicating the quality of the film. The obtained L_φ shows a strong temperature dependence as shown in Figure 4b. The coherence length increases with decreasing temperature, saturating at ~380 nm. The observed saturation of L_φ may result from strong electron-electron interaction in the low temperature regime[44,45]. A power law fit of the coherence length at low temperatures shows $L_\varphi \sim T^{-0.44}$ dependence (inset to Figure 4b). In general, a power law dependence of $T^{-0.50}$ represents a 2-dimensional (2D) system, while $T^{-0.75}$ represents a 3-dimensional (3D) system[44]. Hence, the observed temperature dependence of L_φ suggests that the WAL at low temperatures could possibly originate from a 2D surface state. Although the transport measurements reveal useful parameters such as $\alpha \approx 0.5$ and $L_\phi \approx 380$ nm, consistent with previous studies on Bi_2Se_3 [52] and other TIs [41,43], it does not demonstrate that the observed WAL originates exclusively from the TSS; the magneto-transport response could be due to coupling of the top and bottom TSS through the bulk or could be due to a significant response from the top TSS. In both cases, however, $\alpha = 0.5$, is consistent with the presence of topological surface state(s), though we can't exclude the possibility of bulk (and QWS) interference in the transport measurements (see Supplemental Material for high field magnetoresistance up to 7 T, exhibiting a certain degree of non-linearity). In our case, we estimate the magnetic field would have to be raised to ≈ 40 T to observe the first SdH oscillation (from the condition $\mu B > 1$ for closed orbits, Hall transport mobility is 246 $cm^2/V\bullet s$), which could provide further information about the surface transport. The THz measurements on the other hand, clearly shows a TSS response at low temperature and a gradual transition to the bulk and QWS at temperatures > 30K, demonstrating the surface sensitive advantage provided by the THz measurement over the transport measurement.

In conclusion, our experimental results provide evidence for the existence of a TSS at low temperature in a 23-QL-thick Bi_2Se_3 thin film using THz spectroscopy. The temperature dependence of the THz mobility and scattering lifetime demonstrate the presence of a metallic TSS below 30 K, reaching a value of ~2100 $cm^2/V.s$ and 0.18 ps respectively, at 4 K. We further elucidate the bulk-to-surface relaxation mechanism which suppresses the increase of the surface scattering rate above 50 K. However below 50 K, the relaxation is quenched leading to a sharp rise in mobility, characteristic of the TSS. The ability of THz spectroscopy to discriminate surface state from bulk behavior demonstrates the strength of the technique in contrast to Hall measurements. In addition, the Fermi level is estimated to be around 0.38 eV above the Dirac point with the Fermi wave vector $\sim 0.1\ Å^{-1}$,

consistent with ARPES measurements. The direct coupling between the optical radiation in the THz frequency range and the TSS opens up the possibility of developing novel TI devices such as room temperature photodetectors[46] and THz modulators[49] operational in the THz gap. Our work presents a non-destructive method to explore their properties at THz frequencies in a contact-free manner. Furthermore, it is potentially a step towards investigating the TSS at the interfaces of TI-heterostructures – a regime which is difficult to access due to the complex fabrication steps involved, but which can be easily studied using our THz transmission technique. We further show that magneto-transport reveals WAL at low temperatures giving $\alpha \approx 0.5$ which indicates coupling of the top and bottom TSS with a coherence length dependence of $\sim T^{-0.44}$, suggesting a surface state related nature of the charge carriers. The significance of this work was to demonstrate the presence of the TSS in Bi_2Se_3 as a representative example of a general method for the study of Dirac surface behavior in a much wider class of topological materials.

METHODS

Terahertz time domain spectroscopy: Broadband terahertz time domain spectroscopy was carried out on the 23-QL-thick Bi_2Se_3 film with a Tera K15- T-Light MENLO system. The THz (and transport) measurements were carried out within 7 days of the MBE growth of the film. Pulses from a 60-mW pump laser of 90 fs duration at 1560 nm (repetition rate of 100 MHz) were split into two paths: (i) a component focused down to a 40 μm spot onto the THz emitter, resulting in a broadband THz emission with a spot size of ~1 mm (shown in purple), and (ii) a component through the delay stage for THz detection (shown in red). The sample was mounted in a Janis continuous flow cryostat with optical access with a base temperature of 4 K, to obtain a temperature-dependent THz response. See Figure 1a for a schematic of the optical setup. In the ultrathin-film limit, THz conductance spectra are obtained from the normalized transmission using the Tinkham's formulae[25] given as $\tilde{\sigma}(\omega) = \frac{(n_S+1)}{Z_0 d_f}\left(\frac{1}{T(\omega)} - 1\right)$, where $T(\omega)$ is the substrate normalized complex transmission amplitude, Z_0 is the vacuum impedance, while n_S is the refractive index of the substrate (3.08). The conductance of thin film is given by $G = \tilde{\sigma} d_f$, where $\tilde{\sigma}$ is the optical conductivity and d_f is the thickness of the film.

Bi_2Se_3 growth: Molecular beam epitaxy (MBE) was used to grow 23 QLs (1 QL = 0.954 nm) of Bi_2Se_3 on a c-plane sapphire (0001) substrate. The base pressure in our UHV system was $1x10^{-10}$ Torr. Effusion cells were used to evaporate [Bi (6N) and Se (6N)] high-purity source materials. A two-step growth procedure was followed to ensure uniform growth: A seed layer of ~5 nm thickness was grown at a substrate temperature of 250°C, which was followed by an annealing stage with the substrate temperature raised up to 300°C. This process reduces twinning[47], commonly observed in this materials system. The Bi:Se flux ratio, recorded by an *in-situ* beam flux monitor, was 1:10. The final 21.9-nm-thick Bi_2Se_3 layer was grown keeping the substrate at the same temperature of 300°C.

Device fabrication and electrical transport: Optical-lithography was used to define a microscale Hall bar of dimensions 1400 μm × 80 μm. This was followed by the deposition of 15 nm Ti and 90 nm Au and a standard lift-off process to obtain ohmic contacts to the mesa. The device was then packaged and measured in a He-3 cryostat with a base temperature of 300 mK. Hall measurements were obtained using an a.c lock-in four-terminal setup with an input current of 1 μA at a frequency of 133 Hz.

ASSOCIATED CONTENT

Supporting information: XRD and XRR measurements to characterize the quality, phase and thickness of the Bi_2Se_3 film; field dependence of the longitudinal and Hall resistance measurement at corresponding temperatures; THz time domain response of the (0001)-oriented sapphire substrate at

different temperatures.

AUTHOR INFORMATION NOTES

Corresponding author
*E-mail: vk302@cam.ac.uk

ORCID
Varun. S. Kamboj: 0000-0003-0874-551X
Angadjit Singh: 0000-0003-4922-4956
Thierry Ferrus: 0000-0002-9887-3509
Liam B. Duffy: 0000-0001-6842-4094
Thorsten Hesjedal: 0000-0001-7947-3692
Harvey. E. Beere: 0000-0001-5630-2321
Crispin. H. W. Barnes: 0000-0001-7337-7245
David. A. Ritchie: 0000-0002-9844-8350

Notes
The authors declare no competing financial interest.
Additional data sets related to this publication are available from the Cambridge University data repository at https://doi.org/10.17863/CAM.11276.

ACKNOWLEDGMENTS

V.S.K., H.E.B., and D.A.R. acknowledge financial support from the Engineering and Physical Sciences Research Council (EPSRC) (Grant No. EP/J017671/1, Coherent Terahertz Systems). V.S.K., and A.S. also acknowledge financial support Cambridge Commonwealth Trust. T.H. acknowledges financial support from John Fell Oxford University Press Research Fund. L.B.D. would like to acknowledge the financial support from EPSRC and the Science and Technology Facilities Council (UK). T.F. acknowledges support from the Project for Developing Innovation Systems of the Ministry of Education, Culture, Sports, Science and Technology (MEXT), Japan.

REFERENCES

(1) Hasan, M. Z.; Kane, C. L. Colloquium: Topological insulators. *Rev. Mod. Phys.* **2011,** *82*, 3045–3067.
(2) Hasan, M. Z.; Moore, J. E. Three-Dimensional Topological Insulators. *Annu. Rev. Condens. Matter Phys*. **2011,** *2*, 55-78.
(3) Qi, X. L.; Zhang S. C. Topological insulators and superconductors. *Rev. Mod. Phys.* **2011,** *83***,** 1057.
(4) Fu. L,; Kane, C. L; Mele, E. J. Topological Insulators in Three Dimensions. *Phys. Rev. Lett.* **2007**, *98*, 106803.
(5) Moore, J. E.; Balents. L. Topological invariants of time-reversal-invariant band structures. *Phys. Rev. B*. **2007,** *75*, 121306.
(6) Xia, Y.; Qian, D.; Hsieh, D.; Wray, L.; Pal, A.; Lin, K.; Bansil, A.; Grauer, A.; Cava, R. J.; Hasan, M. Z. Observation of a large-gap topological-insulator class with a single Dirac cone on the surface. *Nat. Phys.* **2009,** *5*, 398-402.
(7) Zhang, H.; Liu, C. X.; Qi, X.-L.; Dai, X.; Fang, Z.; Zhang, S. C. Topological Insulators in Bi_2Se_3, Bi_2Te_3 and Sb_2Te_3 with a Single Dirac Cone on the Surface. *Nat. Phys.* **2009**, *5*, 438–442.
(8) Hsieh, D.; Xia, Y.; Qian, D.; Wray, L.; Meier, F.; Dil, J.H.; Osterwalder, J.; Patthey, L.; Fedorov, A.V.; Lin, H.; Bansil, A.; Grauer, D.; Hor, Y. S; Cava, R. J.; Hasan, M. Z. Observation of Time-Reversal-Protected Single-Dirac-Cone Topological-Insulator States in Bi_2Se_3 and Sb_2Te_3. *Phys. Rev. Lett.* **2009**, *103*, 146401.
(9) Chen, Y. L.; Analytis, J. G.; Chu, J. H.; Liu, Z. K.; Mo, S. K.; Qi, X. L.; Zhang, H. J.; Lu, D. H.; Dai, X.; Fang, Z.; Zhang, S. C.; Fisher, I. R.; Hussain, Z.; Shen, Z. X. Experimental Realization of a Three-Dimensional Topological Insulator, Bi_2Te_3. *Science* **2009,** *325*, 178-181.
(10) Kane, C. L.; Mele, E. J. Z_2 Topological Order and the Quantum Spin Hall Effect. *Phys. Rev.*

Lett. **2005**, *95*, 146802.
(11) Liu, C. X.; Qi, X. L.; Zhang, H. J.; Dai, X.; Fang, Z.; Zhang, S. C. Model Hamiltonian for topological insulators. *Phys. Rev. B.* **2010,** *82*, 045122.
(12) Fu, L.; Kane, C. L. Superconducting Proximity Effect and Majorana Fermions at the Surface of a Topological Insulator. *Phys. Rev. Lett.* **2008**, *100*, 096407.
(13) Hsieh, D.; Qian, D.; Wray, L.; Xia, Y.; Hor, Y. S.; Cava, R. J.; Hasan, M. Z. A topological Dirac insulator in a quantum spin Hall phase. *Nature* **2008,** *452*, 970–974.
(14) Brahlek, M.; Kim, Y. S.; Bansal, N.; Edrey, E.; Oh, S. Surface versus bulk state in topological insulator Bi_2Se_3 under environmental disorder. *Appl. Phys. Lett.* **2011**, *99*, 012109.
(15) Bianchi, M.; Guan, D.; Bao, S.; Mi, J.; Iversen, B.; King, P.; Hofmann, P. Coexistence of the topological state and a two-dimensional electron gas on the surface of Bi_2Se_3. *Nat. Commun.* **2010**, *1*, 128.
(16) King, P. D. C.; Hatch, R. C.; Bianchi, M.; Ovsyannikov, R.; Lupulescu, C.; Landolt, G.; Slomski, B.; Dil, J. H.; Guan, D.; Mi, J. L.; Rienks, E. D. L.; Fink, J.; Lindblad, A.; Svensson, S.; Bao, S.; Balakrishnan, G.; Iversen, B. B.; Osterwalder, J.; Eberhardt, W.; Baumberger, F.; Hofmann, P. Large Tunable Rashba Spin Splitting of a Two-Dimensional Electron Gas in Bi_2Se_3. *Phys. Rev. Lett.* **2011**, *107*, 096802.
(17) Valdés Aguilar, R.; Qi, J.; Brahlek, M.; Bansal, N.; Azad, A.; Bowlan, J.; Oh, S.; Taylor, A. J.; Prasankumar, R. P.; Yarotski, D. A. Time-Resolved Terahertz Dynamics in Thin Films of the Topological Insulator Bi_2Se_3. *Appl. Phys. Lett.* **2015**, *106*, 011901.
(18) Tang, C. S.; Xia, B.; Zou, X.; Chen, S.; Ou, H. W.; Wang, L.; Rusydi, A.; Zhu, J. X.; Chia, E. E. M. Terahertz Conductivity of Topological Surface States in $Bi_{1.5}Sb_{0.5}Te_{1.8}Se_{1.2}$. *Sci. Rep.* **2013**, *3*, 3513.
(19) Yashina, L.; Sánchez-Barriga, J.; Scholz, M. R.; Volykhov, A. A.; Sirotina, A. P.; Neudachina, V. S.; Tamm, M. E.; Varykhalov, A.; Marchenko, D.; Springholz, G.; Bauer, G.; Knop-Gericke, A.; Rader. O. Negligible Surface Reactivity of Topological Insulators Bi_2Se_3 and Bi_2Te_3 Towards Oxygen and Water. *ACS Nano* **2013**, *7*, 5181.
(20) Richardella, A.; Zhang, D. M.; Lee, J. S.; Koser, A.; Rench, D. W.; Yeats, A. L.; Buckley, B. B.; Awschalom, D. D.; Samarth, N. Coherent Heteroepitaxy of Bi_2Se_3 on GaAs (111)B. *Appl. Phys. Lett.* **2010**, *97*, 262104.
(21) Wang, E.; Ding, H.; Fedorov, A. V.; Yao, W.; Li, Z.; Lv, Y.-F.; Zhao, K.; Zhang, L.-G.; Xu, Z.; Schneeloch, J.; Zhong, R.; Ji, S.-H.; Wang, L.; He, K.; Ma, X.; Gu, G.; Yao, H.; Xue, K.-M.; Chen, X.; Zhao, S. Fully Gapped Topological Surface States in Bi_2Se_3 Films Induced by a D-Wave High-Temperature Superconductor. *Nat. Phys.* **2013**, *9*, 621–625.
(22) Benia, H. M.; Lin, C.; Kern, K.; Ast, C. R. Reactive Chemical Doping of the Bi_2Se_3 Topological Insulator. *Phys. Rev. Lett.* **2011**, *107*, 177602.
(23) Park, B. C.; Kim, T. H.; Sim, K. I.; Kang, B.; Kim, J. W.; Cho, B.; Jeong, K. H.; Cho, M. H.; Kim, J. H. Terahertz Single Conductance Quantum and Topological Phase Transitions in Topological Insulator Bi_2Se_3 Ultrathin Films. *Nat. Commun.* **2015**, *6*, 6552.
(24) Valdés Aguilar, R.; Stier, A. V.; Liu, W.; Bilbro, L. S.; George, D. K.; Bansal, N.; Wu, L.; Cerne, J.; Markelz, A. G.; Oh, S.; Armitage. N. P. Terahertz Response and Colossal Kerr Rotation from the Surface States of the Topological Insulator Bi_2Se_3. *Phys. Rev. Lett.* **2012**, *108*, 087403.
(25) Nuss, M. C.; Orenstein, J.; *Millimeter and Submillimeter Wave Spectroscopy of Solids*. Springer-Verlag Berlin Heidelberg, 1998; pp 7-50.
(26) Bansal, N.; Kim, Y. S.; Brahlek, M.; Edrey, E.; Oh, S. Thickness-Independent Transport Channels in Topological Insulator Bi_2Se_3 Thin Films. *Phys. Rev. Lett.* **2012**, *109*, 116804.
(27) He, L.; Xiu, F.; Yu, X.; Teague, M.; Jiang, W.; Fan, Y.; Kou, X.; Lang, M.; Wang, Y.; Huang, G.; Nai-Chang, Y.; Wang, K. L. Surface-Dominated Conduction in a 6 nm thick Bi_2Se_3 Thin Film. *Nano Lett.* **2012**, *12*, 1486–1490.
(28) Yu, P. Y.; Cardona, M. Fundamentals of Semiconductors: Physics and Materials Properties, 3rd ed.; Springer-Verlag: Berlin Heidelberg, 2010; pp 220-223.
(29) Sobota, J. A.; Yang, S.; Analytis, J. G.; Chen, Y. L.; Fisher, I. R.; Kirchmann, P. S.; Shen, Z. X. Ultrafast Optical Excitation of a Persistent Surface-State Population in the Topological Insulator Bi_2Se_3. *Phys. Rev. Lett.* **2012**, *108*, 117403.
(30) Hajlaoui, M.; Papalazarou, E.; Mauchain, J.; Lantz, G.; Moisan, N.; Boschetto, D.; Jiang, Z.; Miotkowski, I.; Chen, Y. P.; Taleb-Ibrahimi, A; Perfetti. L.; Marsi. M. Ultrafast Surface Carrier Dynamics in the Topological Insulator Bi_2Te_3. *Nano Lett.* **2012**, *12*, 3532–3536.
(31) Wang, Y. H.; Hsieh, D.; Sie, E. J.; Steinberg, H.; Gardner, D. R.; Lee, Y. S.; Jarillo-Herrero, P.; Gedik,

N. Measurement of Intrinsic Dirac Fermion Cooling on the Surface of the Topological Insulator Bi_2Se_3 Using Time-Resolved and Angle-Resolved Photoemission Spectroscopy. *Phys. Rev. Lett.* **2012**, *109*, 127401.

(32) Sim, S.; Brahlek, M.; Koirala, N.; Cha, S.; Oh, S.; Choi, H. Ultrafast Terahertz Dynamics of Hot Dirac-Electron Surface Scattering in the Topological Insulator Bi_2Se_3. *Phys. Rev. B.* **2014**, *89*, 165137.

(33) Analytis, J. G.; Chu, J. H.; Chen, Y.; Corredor, F.; McDonald, R. D.; Shen, Z. X.; Fisher, I. R. Bulk Fermi Surface Coexistence with Dirac Surface State in Bi_2Se_3: A Comparison of Photoemission and Shubnikov-de Haas Measurements. *Phys. Rev. B.* **2010**, *81*, 205407.

(34) Butch, N. P.; Kirshenbaum, K.; Syers, P.; Sushkov, A. B.; Jenkins, G. S.; Drew, H. D.; Paglione, J. Strong Surface Scattering in Ultrahigh-Mobility Bi_2Se_3 Topological Insulator Crystals. *Phys. Rev. B.* **2010**, *81*, 241301.

(35) Brahlek, M.; Koirala, N.; Salehi, M.; Bansal, N.; Oh, S. Emergence of Decoupled Surface Transport Channels in Bulk Insulating Bi_2Se_3 Thin Films. *Phys. Rev. Lett.* **2014**, *113*, 026801.

(36) Wray, L. A.; Xu, S.; Xia, Y.; Hor, Y. S.; Qian, D.; Fedorov, A. V; Lin, H.; Bansil, A.; Cava, R. J.; Hasan, M. Z. Observation of Topological Order in a Superconducting Doped Topological Insulator. *Nat. Phys.* **2010**, *6*, 855–859.

(37) Waitkins, G. R.; Shutt, R.; Kinney, I. W.; McReynolds, J. P.; *Inorganic syntheses*. Vol. 2. John Wiley & Sons, Inc., Hoboken, 1946; pp 183-186.

(38) Chen, C.; He, S.; Weng, H.; Zhang, W.; Zhao, L.; Liu, H.; Jia, X.; Mou, D.; Liu, S.; He, J.; Peng, Y.; Feng, Y.; Xie, Z.; Liu, G.; Dong, X.; Zhang, J.; Wang, X.; Peng, Q.; Wang, Z.; Zhang, S.; Yang, F.; Chen, C.; Xu, Z.; Dai, X.; Fang, X.; Zhou, X. J. Robustness of Topological Order and Formation of Quantum Well States in Topological Insulators Exposed to Ambient Environment. *Proc. Natl. Acad. Sci.* **2012**, *109*, 3694–3698.

(39) Chen, J.; He, X. Y.; Wu, K. H.; Ji, Z. Q.; Lu, L.; Shi, J. R.; Smet, J. H.; Li, Y. Q. Tunable Surface Conductivity in Bi_2Se_3 Revealed in Diffusive Electron Transport. *Phys. Rev. B.* **2011**, *83*, 241304.

(40) Hikami, S.; Larkin, A. I.; Nagaoka, Y. Spin-Orbit Interaction and Magnetoresistance in the Two Dimensional Random System. *Prog. Theor. Phys.* **1980**, *63*, 707–710.

(41) Nguyen, T.; Backes, D.; Singh, A.; Mansell, R.; Barnes, C.; Ritchie, D.; Mussler, G.; Lanius, M.; Grützmacher, D.; Narayan, V. Topological States and Phase Transitions in Sb_2Te_3-GeTe Multilayers. *Sci. Rep.* **2016**, 27716.

(42) Veldhorst, M.; Snelder, M.; Hoek, M.; Molenaar, C. G.; Leusink, D. P.; Golubov, A. A.; Hilgenkamp, H.; Brinkman, A. Magnetotransport and Induced Superconductivity in Bi Based Three-Dimensional Topological Insulators. *Phys. Status Solidi - Rapid Res. Lett.* **2013**, *7*, 26–38.

(43) He, H. T.; Wang, G.; Zhang, T.; Sou, I. K.; Wong, G. K. L.; Wang, J. N.; Lu, H. Z.; Shen, S. Q.; Zhang, F. C. Impurity Effect on Weak Antilocalization in the Topological Insulator Bi_2Te_3. *Phys. Rev. Lett.* **2011**, *106*, 166805.

(44) Altshuler, B. L.; Aronov, A. G.; Khmelnitsky, D. E. Effects of Electron-Electron Collisions with Small Energy Transfers on Quantum Localisation. *J. Phys. C Solid State Phys.* **1982**, *15*, 7367–7386.

(45) Assaf, B. A.; Cardinal, T.; Wei, P.; Katmis, F.; Moodera, J. S.; Heiman, D. Linear Magnetoresistance in Topological Insulator Thin Films: Quantum Phase Coherence Effects at High Temperatures. *Appl. Phys. Lett.* **2013**, *102*, 012102.

(46) Viti, L.; Coquillat, D.; Politano, A.; Kokh, K. A.; Aliev, Z. S.; Babanly, M. B.; Tereshchenko, O. E.; Knap, W.; Chulkov, E. V.; Vitiello, M. S. Plasma-Wave Terahertz Detection Mediated by Topological Insulators Surface States. *Nano Lett.* **2016**, *16*, 80–87.

(47) Harrison, S. E.; Li, S.; Huo, Y.; Zhou, B.; Chen, Y. L.; Harris, J. S. Two-Step Growth of High Quality Bi_2Te_3 Thin Films on Al_2O_3 (0001) by Molecular Beam Epitaxy. *Appl. Phys. Lett.* **2013**, *102*, 171906.

(48) Kumar, D.; Lakhani, A. Observation of π Berry phase in quantum oscillations of three-dimensional Fermi surface in topological insulator Bi_2Se_3. *Phys. Status Solidi - Rapid Res. Lett.* **2015**, *9*, 636–640.

(49) Sim, S.; Jang, H.; Koirala, N.; Brahlek, M.; Moon, J.; Sung, J. H.; Park, J.; Cha, S.; Oh, S.; Jo, M.; Ahn, J.; Choi, H. Ultra-High Modulation Depth Exceeding 2,400% in Optically Controlled Topological Surface Plasmons. *Nat. Commun.* **2015**, *6*, 8814.

(50) Valdés Aguilar, R.; Qi, J.; Brahlek, M.; Bansal, N.; Azad, A.; Bowlan, J.; Oh, S.; Taylor, A. J.; Prasankumar, R. P.; Yarotski, D. A. Time-Resolved Terahertz Dynamics in Thin Films of the Topological Insulator Bi_2Se_3. *Appl. Phys. Lett.* **2015**, 106, 011901.

(51) Qi, J.; Chen, X.; Yu, W.; Cadden-Zimansky, P.; Smirnov, D.; Tolk, N. H.; Miotkowski, I.; Cao, H.; Chen, Y. P.; Wu, Y.; Qiao, S.; Jiang, Z. Ultrafast Carrier and Phonon Dynamics in Bi_2Se_3 Crystals. *Appl. Phys. Lett.* **2010**, *97*, 182102.

(52) Chen, J.; Qin, H. J.; Yang, F.; Liu, J.; Guan, T.; Qu, F. M.; Zhang, G. H.; Shi, J. R.; Xie, X. C.; Yang, C. L.; Wu, K. H.; Li, Y. Q.; Lu. L. Gate-Voltage Control of Chemical Potential and Weak Antilocalization in Bi_2Se_3. *Phys. Rev. Lett.* **2010**, *105*, 176602.
(53) Steinberg, H.; Lalo, J.; Fatemi, V.; Moodera, J. S.; Herrero, P. J. Electrically Tunable Surface-to-Bulk Coherent Coupling in Topological Insulator Thin Films. *Phys. Rev. Lett.* **2011**, 84, 233101